

Vision-Based Sensing and Control for Space Robotics Applications

Michael E. Stieber, *Member, IEEE*, Michael McKay, George Vukovich, *Member, IEEE*, and Emil Petriu, *Senior Member, IEEE*

Abstract—The following problems arise in the precise positioning of payloads by space manipulators:

- 1) the precise measurement of the relative position and motion of objects in the workspace of the robot;
- 2) the design of a control system, which is robust and performs well in spite of the effects of structural flexibility and oscillations typically associated with space robots.

This paper discusses the solution to the measurement problem by a vision system using photogrammetric image processing to determine the motion of objects in real time. Performance characteristics are presented. The control problem is addressed by a new technique dealing effectively with the challenge posed by the noncollocated sensor/actuator configuration on the flexible robot structure. The laboratory implementation of the measurement and control concepts is discussed. Preliminary results validate the concepts.

Index Terms—Artificial vision, control, measurement of motion, photogrammetry, robotics.

I. INTRODUCTION

ROBOTIC systems will play an important role in reducing hazards and increasing productivity of humans in space. A prime example is the Mobile Servicing System (MSS) shown in Fig. 1 which is presently being developed by the Canadian Space Agency for the assembly and external maintenance of the International Space Station (ISS) [1]. As the tasks performed by space robots become more complex, the need for more human-like characteristics emerges. As with humans, the sense of sight is essential to enabling efficient interaction with the environment. More important than the sense of sight per se is the ability to process images in such a way as to enable more efficient, accurate and autonomous control of the robot.

This paper addresses measurement and control problems associated with the precise positioning of large space robot manipulators like the Space Station Remote Manipulator System (SSRMS) shown in Fig. 1, which typically have a very high payload-to-manipulator mass ratio (e.g. 116 000 kg/1500 kg for SSRMS) and relatively low stiffness, resulting in highly time-variant dynamic behavior with significant low-frequency oscillations. A theoretical concept for the systematic design of an instrumentation architecture for such systems

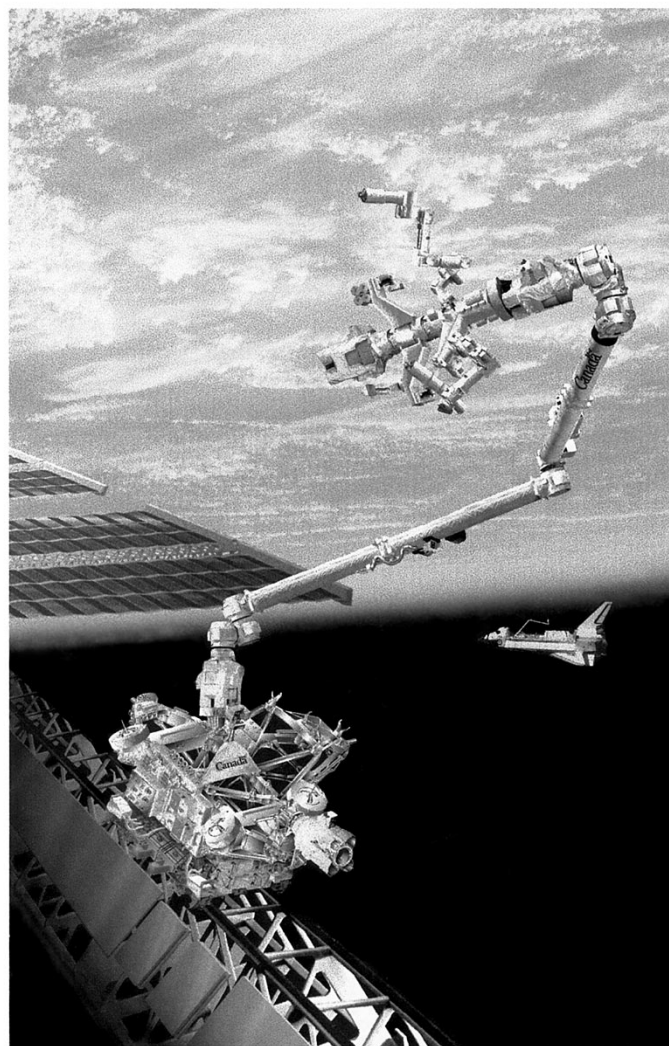


Fig. 1. Mobile Servicing System on the International Space Station.

was presented in [2]. This paper discusses the experimental implementation and evaluation of this concept in a laboratory setting. Section II discusses the measurement of the manipulator payload motion, including the contributions due to structural flexibility, relative to other objects in the manipulator workspace using a vision system. In Section III we extend the theoretical concept of [2] to the case of partially noncollocated sensor/actuator configurations on flexible structures and discuss the design and performance of a control system for the laboratory robot.

Manuscript received May 23, 1996; revised April 12, 1999.

M. E. Stieber and G. Vukovich are with the Canadian Space Agency, St. Hubert, P.Q., Canada.

M. McKay is with the Department of National Defense, Ottawa, Ont., Canada.

E. Petriu is with the University of Ottawa, Ottawa, Ont., K1N 6N5, Canada.

Publisher Item Identifier S 0018-9456(99)06676-0.

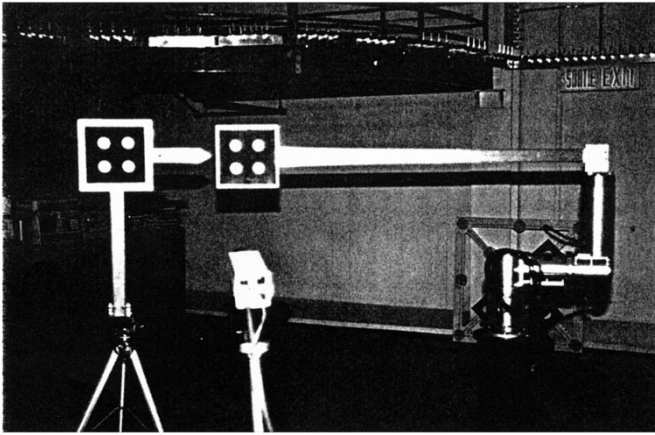


Fig. 2. Experimental robot.

II. VISION-BASED MEASUREMENT SYSTEM

A. Experimental Set-Up

The objective of our experimental work is to develop, evaluate and demonstrate concepts for vision-based sensing and control for space robotics applications. The robot shown in Fig. 2 is specifically designed to emulate certain dynamic characteristics of a space robot such as the SSRMS. The robot has three revolute joints and a very flexible link to which various payloads can be attached, affecting considerably the dynamic behavior of the system. The joints are actuated by dc motors with harmonic drives and are instrumented with tachometers and encoders. One particular objective is to demonstrate the rapid and precise positioning of payloads with respect to a berthing site in the workspace which roughly measures $1.5 \times 1.5 \times 1 \text{ m}^3$. The low fundamental frequencies and structural deformations of the flexible beam present significant challenges. The vision system used in the laboratory is functionally equivalent to the Space Vision System (SVS) successfully flown on the Space Shuttle in 1992 and 1995 [3]. A next-generation SVS being developed by the Canadian Space Agency will support robotic assembly operations on the International Space Station. The setup in the laboratory shown in Fig. 3 is in principle similar to that for a space mission. A single video camera is used to image the robot workspace, which includes dedicated visual targets. The relative position, orientation and velocity between the robot "Payload" and its "Berth" to which it is to be maneuvered, are determined by image processing.

B. Measurement of Position and Orientation

The various points and associated coordinate frames used by the vision system are identified in Fig. 4, which also defines abbreviations for long names. The relative position and orientation of the various reference frames can be conveniently described by homogeneous coordinate transformations, defined by transformation matrices $\mathbf{T} \in \mathbb{R}^{4 \times 4}$ [4]. The transformation ${}^A_B\mathbf{T}$ transforms the coordinates of a point expressed in reference frame A into the coordinates in frame B . The inverse

transformation for going from B to A is ${}^B_A\mathbf{T} = {}^A_B\mathbf{T}^{-1}$ and always exist.

Our goal is to determine the relative position and orientation between Berth and Payload in order to provide a guidance command to the robot. This transformation can be expressed in terms of a chain of homogeneous transformations

$${}^{\text{Berth}}_{\text{Payload}}\mathbf{T} = {}^{\text{Berth}}_{\text{Cam}}\mathbf{T} \cdot {}^{\text{Cam}}_{\text{PTarget}}\mathbf{T} \cdot {}^{\text{PTarget}}_{\text{Payload}}\mathbf{T}. \quad (1)$$

The transformation ${}^{\text{Berth}}_{\text{Cam}}\mathbf{T}$ is given by

$${}^{\text{Berth}}_{\text{Cam}}\mathbf{T} = {}^{\text{Berth}}_{\text{O}}\mathbf{T}^{-1} \cdot {}^{\text{O}}_{\text{CamB}}\mathbf{T} \cdot {}^{\text{CamB}}_{\text{PTU}}\mathbf{T} \cdot {}^{\text{PTU}}_{\text{CamH}}\mathbf{T} \cdot {}^{\text{CamH}}_{\text{Cam}}\mathbf{T}. \quad (2)$$

The transformation ${}^{\text{Cam}}_{\text{PTarget}}\mathbf{T}$ in (1) is determined by photogrammetric image processing as discussed in detail below, while the other transformations on the right-hand side of (1) must be "known" *a priori* in order to determine the left-hand side. Transformations ${}^{\text{PTarget}}_{\text{Payload}}\mathbf{T}$, ${}^{\text{Berth}}_{\text{O}}\mathbf{T}$, ${}^{\text{CamH}}_{\text{Cam}}\mathbf{T}$ can be accurately measured "before flight" and are not subject to significant variations "in flight" because of the relatively small translations typically associated with these transformations. Although the transformations ${}^{\text{O}}_{\text{CamB}}\mathbf{T}$ and ${}^{\text{Berth}}_{\text{O}}\mathbf{T}$ can also be measured "before flight," thermal deformations and other effects can lead to variations "in flight" which can be significant in comparison to the accuracy of the SVS. Cameras are often mounted on pan-and-tilt units (PTU's) which provide a read-out of pan and tilt angles, but with insufficient accuracy for our purposes. Hence one has to assume that there is significant uncertainty associated with ${}^{\text{PTU}}_{\text{CamH}}\mathbf{T}$. The effect of all these errors can be reduced considerably by calibration using a stationary auxiliary Berthing Target. After photogrammetric measurement of ${}^{\text{Cam}}_{\text{BerthTarget}}\mathbf{T}$ we can use the following relationship to calibrate the estimate for ${}^{\text{Berth}}_{\text{Cam}}\mathbf{T}$ in (2):

$${}^{\text{Berth}}_{\text{Cam}}\mathbf{T} = {}^{\text{Cam}}_{\text{BerthTarget}}\mathbf{T}^{-1} \cdot {}^{\text{BerthTarget}}_{\text{Berth}}\mathbf{T}^{-1}. \quad (3)$$

C. Photogrammetric Image Processing

Fig. 5 shows the basic relations between the position of a target in the real world and its image on the CCD of an ideal camera with focal length f_e . It is well known [4] that the X , Y , Z coordinates of a particular target element j in real world (\mathbf{P} frame) and its y , z photo-coordinates in the image plane (\mathbf{I} frame) are related as follows:

$$\frac{{}^{\text{Cam}}\mathbf{I}_y(j)}{f_e} = \frac{{}^{\text{Cam}}\mathbf{P}_Y(j)}{{}^{\text{Cam}}\mathbf{P}_X(j)} \quad (4)$$

$$\frac{{}^{\text{Cam}}\mathbf{I}_z(j)}{f_e} = \frac{{}^{\text{Cam}}\mathbf{P}_Z(j)}{{}^{\text{Cam}}\mathbf{P}_X(j)}. \quad (5)$$

Part of the target design is the placement of target elements with respect to each other. Thus the locations of the target elements are known in the payload target reference frame. Based on this *a priori* knowledge, the six unknown parameters of the transformation ${}^{\text{Cam}}_{\text{PTarget}}\mathbf{T}$ can be uniquely determined from (4) and (5) iff the target array has three or more elements, i.e. $j = 1 \dots k, k \geq 3$. The solution of these nonlinear equations requires iterative numerical methods in most cases. The SVS applies small corrections to (4) and (5) in order to compensate for optical imperfections of the

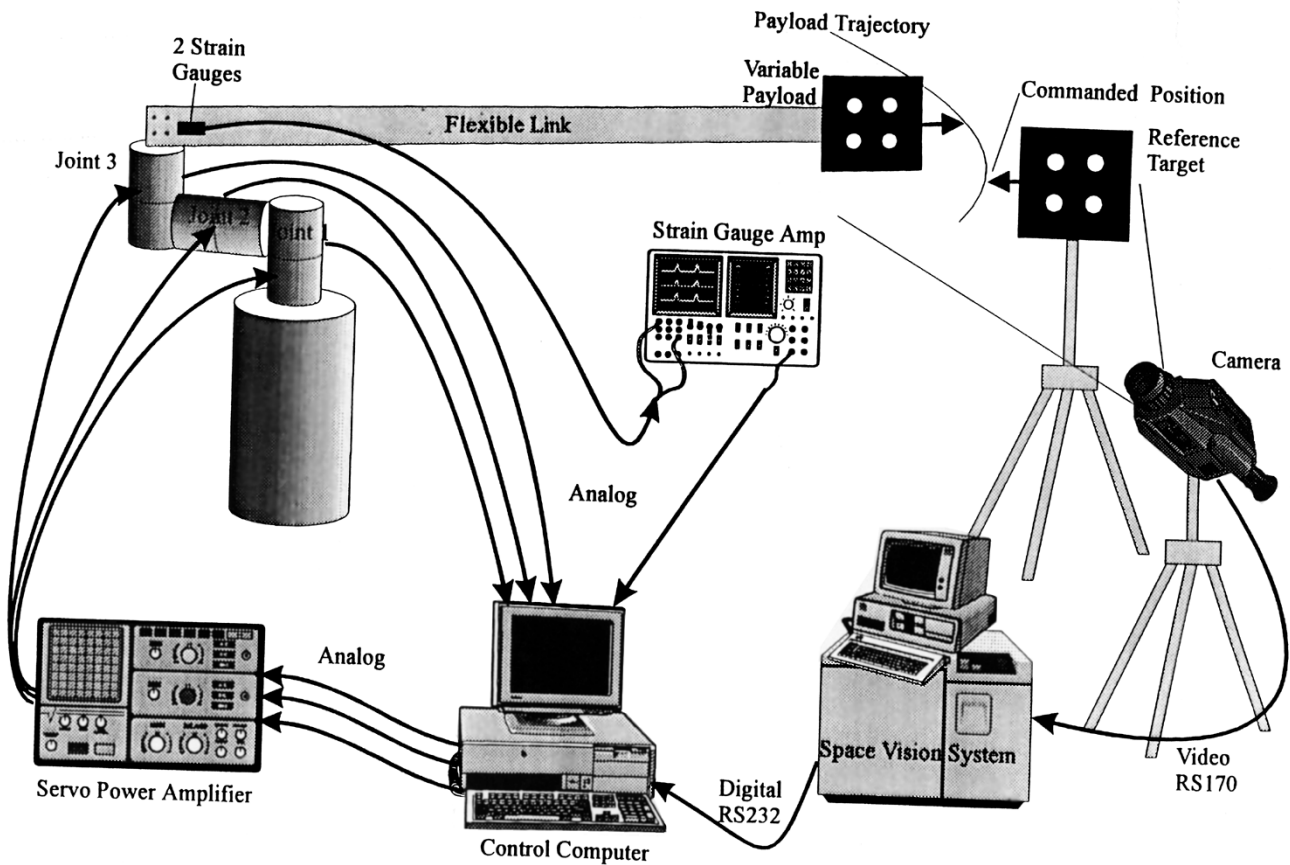


Fig. 3. Experimental setup.

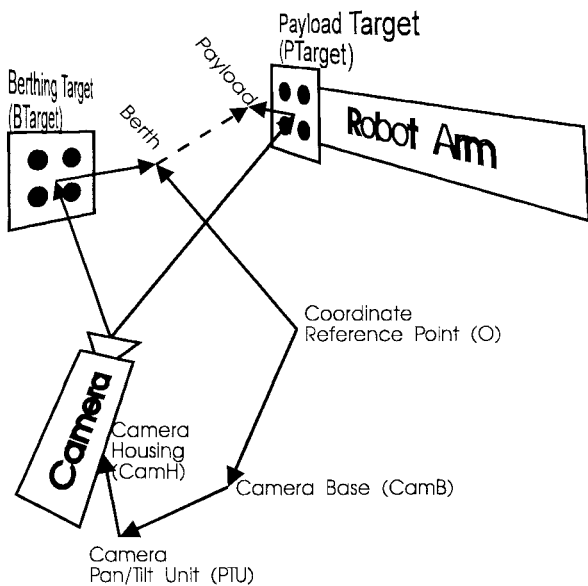


Fig. 4. Reference frames used by vision system.

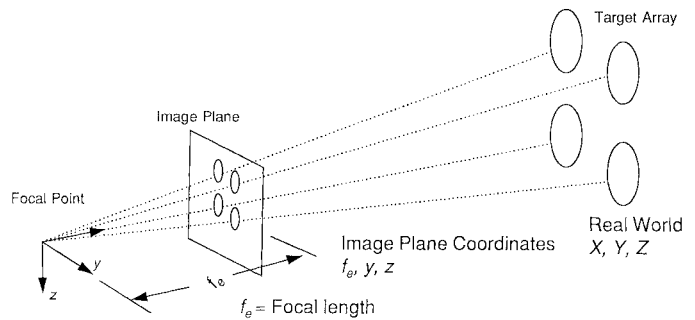


Fig. 5. Photogrammetric relationships.

However, the SVS is also able to track other target elements such as corners, intersections of lines and ends of lines.

As an example for photogrammetric image processing, Fig. 6 shows the motion of one of the payload target elements in the camera image as the payload moves through the workspace. For the same case, Fig. 7 shows the time history of the payload motion in the berth frame, computed by solving (4) and (5) and performing the transformation (1) and (2).

camera/lens assembly, which are determined in a one-time camera calibration process.

The centroid position of each target elements is interpolated to a sub-pixel level to further increase the accuracy of the photogrammetric solution. Due to their symmetries, circular target elements permit very accurate and robust centroid determination and are therefore preferred target elements.

D. Performance Characteristics

Very fast image processing is required in order to support the real-time control of a robotic system. The SVS hosted on a 486 PC computer with C40 DSP boards is capable of processing, at a video frame rate of 30 Hz, the photogrammetric solutions and coordinate transformations for

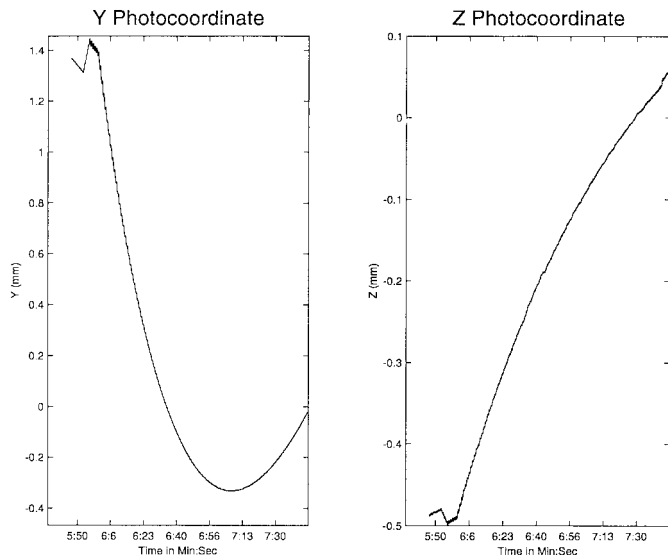


Fig. 6. Camera Image of target motion.

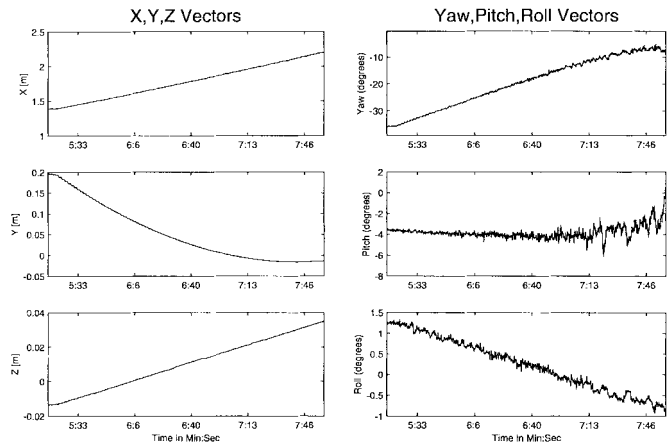


Fig. 7. Payload motion calculated by vision system.

two target arrays with up to ten elements each, using one or two cameras. The measurement accuracies achieved vary considerably with the distance between camera and target, the size and the accuracy of the targets, and the accuracy of the various calibration schemes. During preliminary tests in the laboratory the distance camera–berth was 1.83 m and planar target arrays with four circular dots of 42 mm diameter were used in ambient lighting conditions (Fig. 2). Fig. 8 shows the measurement of the open-loop transient response of the robot with a fundamental frequency of oscillation of 1.1 Hz. The results confirm the ability of the SVS to track the Payload motion in spite of relatively high velocities and accelerations, and to resolve the small components of the motion along the Z -axis and about the roll axis. When the payload is moved through the workspace in a single-joint robot motion, joint-angle encoder measurements can be compared with SVS measurements to estimate the absolute measurement accuracy achieved. Although the geared encoders are considered very accurate, small residual vibrations in the robot flexible structure, which have been identified in the power spectrum of the SVS measurements, introduce some “errors” into this

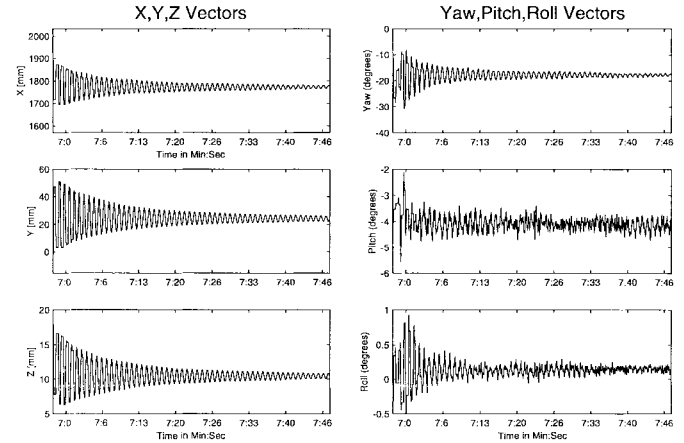


Fig. 8. Robot oscillations tracked by vision systems.

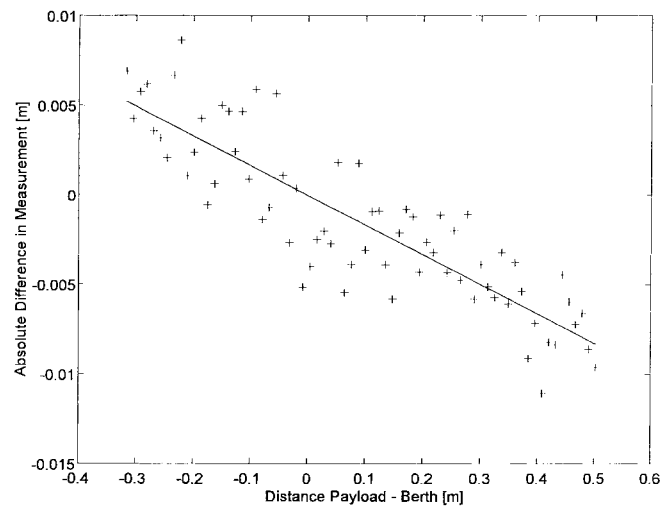


Fig. 9. Differences between SVS and encoder measurements.

comparison. Fig. 9 shows the difference of the payload–berth range measurements by the SVS and the encoder for 70 data points spread over the range of roughly -0.4 m to $+0.5$ m, and a least-squares fit to the data. All measurement differences are less than 10 mm over the entire range. A “systematic error” of about 10 mm/m is observed and attributed to imprecise calibration of the SVS. The “random errors,” which have a standard deviation of 2.3 mm from the regression line, are attributed in part to residual vibrations of the robot and partly to measurement noise in the SVS. The latter could be reduced by filtering the SVS measurements taken at 30 Hz. The robot oscillations could be reduced by more careful experimentation. In spite of their preliminary nature, these results provide confidence in the accuracy of the photogrammetric technique and its suitability for real-time robotics applications.

III. SENSORS AND CONTROL

A. Hyperstability Condition

The approach for defining the overall instrumentation and control architecture for the flexible robot experiment is based on the methodology presented in [2]. This method based on hyperstability theory [5] promises to overcome control system

stability issues associated with the structural flexibility, time-variant dynamics and nonlinearity of the robotic system in a robust manner, and does not require an accurate model of the system dynamics.

In a nutshell, the method requires the selection of sensors and actuators such that the “hyperstability condition” (6) is satisfied. Then a relatively simple control algorithm will robustly stabilize the system in the bounded-input/bounded-output (BIBO) sense [2]

$$\int_{t_0}^{t_1} \mathbf{u}^T(t) \mathbf{y}(t) dt \geq -\gamma_0, \quad \gamma_0 \geq 0 \quad \forall t_1 \geq t_0. \quad (6)$$

In (6), the signals $y_i(t)$ from n sensors were combined to a system output vector $\mathbf{y}(t)$ and the forces and torques $u_i(t)$ applied by n actuators were combined to a system input vector $\mathbf{u}(t)$.

Based on Hamilton’s extended principle and the principle of conservation of energy, condition (6) can be linked to conditions involving the energy transferred by the actuators of electromechanical systems such as the SSRMS and the laboratory robot [2]. In the specific case of the laboratory robot, it follows from the results of [2] that the combination of tachometers and torque motors in the joints satisfies condition (6). The condition can be shown to permit sensor errors such as errors in gain and linearity, saturation effects, noise, bias and dynamic low-pass characteristics.

B. Extension of Instrumentation and Control Concept

However, the measurement of the robot end-point motion by the vision system does not satisfy the sufficient condition (6) and in fact violates necessary conditions on the placement of sensors on flexible structures developed in [2]. It is well known that having “noncollocated” sensors and actuators on a flexible structure gives rise to a variety of problems for active vibration control of the structure [6]. In order to address and solve these problems the concept of [2] is extended by defining a set of m “performance sensors” whose measurement signals z_i are combined to a vector \mathbf{z} . This set includes all sensors necessary to achieve the control objective but do not meet the hyperstability conditions on sensors presented above and in [2]. In the case of the laboratory robot the set of measurements provided by the vision system constitute the performance measurements \mathbf{z} .

Fig. 10 shows a block diagram of the extended concept in which the sensors providing measurements \mathbf{y} which meet the hyperstability condition (6) are now called “hyperstability sensors.” The control signal vector \mathbf{u} is generated by a sensor fusion and control operator \mathbf{C} based on the measurements of the hyperstability sensors \mathbf{y} , the performance sensors \mathbf{z} , and the commanded trajectory or set point vector $\mathbf{w}(t)$:

$$\mathbf{u}(t) = \mathbf{C}\{\mathbf{w}(t), \mathbf{y}(t), \mathbf{z}(t)\}. \quad (7)$$

\mathbf{C} may be composed of algebraic, integral, differential, or fuzzy logic operations on \mathbf{w} , \mathbf{y} , \mathbf{z} . It can be shown that \mathbf{C} will stabilize the system of Fig. 10 in the BIBO sense, if \mathbf{C} satisfies

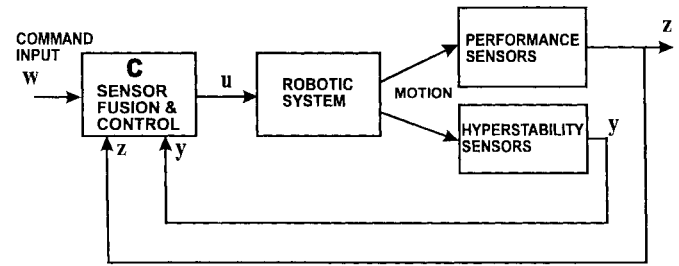


Fig. 10. Extended sensing and control architecture.

the following condition for an arbitrary finite constant $\gamma \geq 0$:

$$\int_{t_0}^{t_1} \mathbf{y}^T \mathbf{C}\{\mathbf{w}, \mathbf{y}, \mathbf{z}\} dt < \gamma \quad \forall t_1 \geq t_0. \quad (8)$$

A particular class of control laws satisfying (8) is given by

$$\mathbf{C} = \begin{cases} \mathbf{C}_1\{\mathbf{w}\} + \mathbf{C}_2\{\mathbf{w}, \mathbf{y}, \mathbf{z}\}, & \text{for } \mathbf{y}^T \mathbf{C}_2\{\mathbf{w}, \mathbf{y}, \mathbf{z}\} < 0 \\ \mathbf{C}_1\{\mathbf{w}\}, & \text{for } \mathbf{y}^T \mathbf{C}_2\{\mathbf{w}, \mathbf{y}, \mathbf{z}\} \geq 0. \end{cases} \quad (9)$$

$\mathbf{C}_1\{\mathbf{w}, \mathbf{y}, \mathbf{z}\}$ in (9) is a feedforward control term, which does not affect the closed-loop stability of the control system as long as it is internally stable. Any knowledge of the dynamic behavior of the robotic system can be used in its construction. $\mathbf{C}_2\{\mathbf{w}, \mathbf{y}, \mathbf{z}\}$ in (9) is a feedback control term, which can be, chosen freely to satisfy the performance objectives of the control system. It can be shown that BIBO stability of the closed-loop system is guaranteed by the logic implied in (9).

C. Control Design for Visual Servoing

Equations (8) and (9) provide a general framework for the design of a control system. We will now see how it can be applied to the laboratory robot by using conventional design approaches. For the clarity of the illustration we pick the simplest situation of controlling the motion of a single joint. The objective is to achieve close tracking of the robot payload position $\mathbf{z}(t)$ to a trajectory $\mathbf{w}(t)$ defined relative to the berthing site in the workspace.

In the case of a scalar system a standard approach to the feedback control problem is PID control [4] as defined below in the frequency domain (s is the Laplace operator, k_P , k_D , k_I are gain constants)

$$\mathbf{C}_2\{\mathbf{w}(s), \mathbf{z}(s)\} = \left(k_P + \frac{k_I}{s} + k_D s \right) (\mathbf{w}(s) - \mathbf{z}(s)). \quad (10)$$

For feedforward control of robots, several methods to determine torque profiles from trajectory commands have been proposed in the robotics literature [4]. As one of our objectives is to demonstrate that our method does not rely on accurate system models we will use a simple lead filter as feedforward, which incorporates only very rudimentary knowledge of the system, such as “which way” to move a joint, but not “how far.” For the simple single-joint case, the lead feedforward control term, with gain and time constants k_1 , k_2 , is defined in the frequency domain as follows:

$$\mathbf{C}_1\{\mathbf{w}(s)\} = \frac{k_1 s}{1 + k_2 s} \mathbf{w}(s). \quad (11)$$

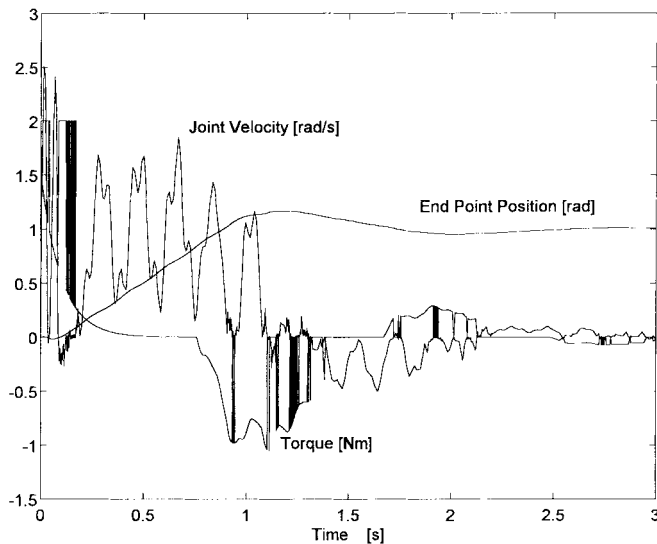


Fig. 11. Simulated motion of laboratory robot.

A particular design for the general control law C is now fully defined by (9)–(11).

Fig. 11 shows a preliminary simulation of the robotic system with the flexible beam and the control system defined above in response to a step function in the trajectory command. The diagram shows a smooth motion of the robot tip and payload which rapidly converges to the new set point of 1 rad within about 2 s. In contrast, the joint motion has a significant oscillatory component due to the flexibility of the link, as indicated by the time history of the joint velocity. Other simulation results have confirmed the robustness of the approach to variations in payload mass and robot dynamic characteristics. Hardware experiments intended to confirm the simulations are in preparation.

IV. SUMMARY AND CONCLUSIONS

Photogrammetric measurement and robot control techniques have been developed for rapid and precise positioning of payloads with flexible space manipulators. Using dedicated visual targets, a vision system provides measurements of the motion of objects in the robot workspace in real time at 30 Hz. The ability of the vision system to track fast moving manipulator motions with sufficient accuracy has been experimentally verified. A control technique was developed which overcomes problems with partially noncollocated sensor/actuator configurations on flexible robots. Simulation results confirm the efficacy and robustness of the control approach.

ACKNOWLEDGMENT

The authors gratefully acknowledge the invaluable assistance of M. Bedirian with the experiments.

REFERENCES

- [1] C. P. Trudel, D. G. Hunter, and M. E. Stieber, "Control and operation of space manipulator systems," in *NATO AGARD Lecture Series 193: Advanced Guidance and Control Aspects in Robotics*, 1993.
- [2] M. E. Stieber, E. Petriu, and G. Vukovich, "Systematic design of instrumentation architecture for complex systems," *IEEE Trans. Instrum. Meas.*, vol. IM-45, Apr. 1996.
- [3] S. G. MacLean and H. F. L. Pinkney, "Machine vision in space," *CASI J.*, vol. 39, no. 2, 1993.
- [4] K. S. Fu, R. C. Gonzales, and C. S. G. Lee, *Robotics: Control Sensing, Vision and Intelligence*. New York: McGraw-Hill, 1987.
- [5] V. M. Popov, *Hyperstability of Control Systems*. Berlin, Germany: Springer-Verlag, 1973.
- [6] V. A. Spector and H. Flashner, "Modeling and design implications of noncollocated control in flexible systems," *Trans. ASME J. Dyn. Syst., Meas., Contr.*, vol. 112, pp. 186–193, June 1990.

Michael E. Stieber (M'88) received the Dipl.-Ing. degree from Technische Universität München, Germany, in 1979 and the Ph.D. degree in electrical engineering from the University of Ottawa, Ottawa, Ont., Canada, in 1998.

He is with the Canadian Space Agency, St. Hubert, P.Q., Canada, currently working on the International Space Station project as Manager, Systems Engineering. He holds several patents on vehicle control systems. His research interests include control systems, instrumentation, robotics and the application of AI techniques to securities trading.

Michael J. McKay, photograph and biography not available at the time of publication.

George Vukovich (M'81) received the Ph.D. degree in electrical engineering from the University of Toronto, Toronto, Ont., Canada, in 1981.

He is Director, Spacecraft Engineering, Canadian Space Agency, St. Hubert, P.Q., Canada, and an Adjunct Professor at the Department of Mechanical and Aerospace Engineering, Carleton University, Ottawa, Ont.

Emil M. Petriu (M'86–SM'88) received the Dipl.Eng. and Dr.Eng. degrees in electrical engineering from the Polytechnic Institute "Traian Vuia," Timisoara, Romania, in 1969 and 1978, respectively.

He has been Professor at the University of Ottawa, Ottawa, Ont., Canada, since 1985 and is currently Director of the School of Information Technology and Engineering (SITE). His research interests include sensors for robotics, neural networks, and fuzzy systems for instrumentation applications and virtual environments. He has co-authored two books, published more than 70 technical papers, and received two patents.

Dr. Petriu is an Associate Editor of this TRANSACTIONS.